

Phase diagrams of Bose-Hubbard model and antiferromagnetic spin-1/2 models on a honeycomb lattice

Takashi Nakafuji and Ikuo Ichinose¹

¹*Department of Applied Physics, Nagoya Institute of Technology, Nagoya, 466-8555, Japan*

(Dated: September 24, 2018)

Motivated by the recent experimental realization of the Haldane model by ultracold fermions in an optical lattice, we investigate phase diagrams of the hard-core Bose-Hubbard model on a honeycomb lattice. This model is closely related with a spin-1/2 antiferromagnetic (AF) quantum spin model. Nearest-neighbor (NN) hopping amplitude is positive and it prefers an AF configurations of phases of Bose-Einstein condensates. On the other hand, an amplitude of the next-NN hopping depends on an angle variable as in the Haldane model. Phase diagrams are obtained by means of an extended path-integral Monte-Carlo simulations. Besides the AF state, a 120°-order state, there appear other phases including a Bose metal in which no long-range orders exist.

PACS numbers: 03.75.Hh, 67.85.Hj, 64.60.De

I. INTRODUCTION

In the recent years, systems of ultracold atomic gases in optical lattices have attracted much attention. Since the systems have the high controllability and versatility, they provide us with a quantum-simulation platform for studying strongly-correlated systems in condensed matter physics, lattice quantum field theories, etc¹. It is established nowadays that low-energy properties of interacting Bose gases in optical lattices are described by the Bose-Hubbard model² and its extension. The idea of quantum simulation by using ultracold atomic systems is also applied to theoretical models that have been regarded as only academic ones. Theoretical predictions for such models are expected to be observed by experiments on ultracold atoms. Recently, generation of artificial gauge fields in ultracold atomic systems in optical lattices was succeeded in the experiments by rotating/shaking optical lattices or by using laser-assisted tunneling^{3,4}. These techniques enable an experimental realization of the Haldane model with ultracold fermions. This model was introduced as a fermionic tight-binding model on a honeycomb lattice that breaks time-reversal symmetry without a net magnetic flux, and it exhibits interesting topological properties as a result of the next-nearest-neighbor (NNN) complex hopping term⁵.

In the present study, we consider a bosonic analog of the Haldane model, which is called Bose-Haldane-Hubbard model (BHHM). A recent study reported its ground-state properties and low-energy excitations at unit filling⁶. In particular, we are interested in the hard-core boson limit where the on-site repulsive interaction U is very large ($U \rightarrow \infty$). We call this model hard-core boson Haldane-Hubbard model (hard-core BHHM). In the previous works^{7,8}, we studied the dipolar hard-core BHHM by means of the extended Monte-Carlo (MC) simulation (see later section) and showed that the model has very rich phase diagrams. In this paper, we study the case in which the nearest-neighbor (NN) hopping amplitude is positive and the NNN hopping is complex depend-

ing on an angle ϕ . Generally, hard-core boson models can be mapped onto spin-1/2 models. The hard-core BHHM is closely related to the quantum spin-1/2 models on the honeycomb lattice. Positive hopping amplitudes in the boson model correspond to antiferromagnetic (AF) exchange couplings in the spin model.

Hard-core BHHM on a small lattice was studied by the exact diagonalization methods⁹. The result suggested that this model had a quantum-liquid state, named Bose metal (BM). The BM corresponds to a gapless spin-liquid state. However, the existence and nature of this state is not established yet. Therefore, it is interesting and also important to study the existence and nature of the BM in larger systems.

In this paper, we shall study the hard-core BHHM on the honeycomb lattice by means of the extended path-integral MC simulations. As stated previously, we take the NN hopping amplitude positive in the present study. In order to study the maximum frustrated case, we also introduce a tunable phase in the NNN hopping such as $J_2 e^{i\phi}$ with $J_2 > 0$. We shall clarify the phase diagrams in the two-dimensional ($\phi - J_2$) plane, etc. Obtained phase diagrams of the BHHM shed light on the properties of the spin-1/2 frustrated AF-XY and AF-XXZ models on the honeycomb lattice. As we mostly consider the case of the half filling, various superfluid (SF) states appear in the phase diagram. Correlation of the phase degrees of freedom of the Bose-Einstein condensate (BEC) has a specific pattern in each SF. Therefore, the terminology of spin is useful to distinguish SFs, and we shall often use it.

The present paper is organized as follows. In Sec. II, we introduce the hard-core BHHM and the path-integral techniques using the slave-particle representation. An effective model is derived by integrating fluctuations in local density as in the previous works^{7,8}. The derived model has a positive-definite action and the MC simulation is applicable for it. In Sec. III, we explain the extended MC simulation by introducing a lattice in the imaginary-time direction. Section IV exhibits the re-

sults of the numerical study. We first study the low-temperature (T) phase diagram of the BHHM with the vanishing NN repulsion and $\phi = 0$. We show that for a small system, the obtained phase diagram is in good agreement with that obtained by the exact diagonalization for the same system size⁹. However, we found that the phase diagrams have rather strong system-size dependence. Besides the expected spin-ordered states, there exists a state that seems to have no long-range orders (LROs), and we call that state BM as in the previous work. We also study the finite- T phase transition. The result indicates that the BM has no LROs. In Sec. V, we study the phase diagrams of the system with various ϕ . Introduction of a finite ϕ diminishes the frustration and stable phases form. Among them, a new phase that we call $\mathbf{k} = (-\pi/\sqrt{3}, 0)$ forms between the AF and 120^o-order states. Finally in Sec. VI, we consider the effect of the NN repulsion, which corresponds to the z -component AF coupling, $\sum S_i^z S_j^z$. Charge density wave (CDW) forms as the NN repulsion is getting large. Section VII is devoted for conclusion.

II. MODEL HAMILTONIAN AND PATH-INTEGRAL FORMULATION

The Hamiltonian of the hard-core BHHM on a honeycomb lattice is given as follows:

$$\begin{aligned} H_{\text{BH}} &= H_0 + H_{\text{NN}}, \\ H_0 &= J_1 \sum_{\langle i,j \rangle} (a_i^\dagger a_j + \text{H.c.}) + J_2 \sum_{\langle\langle i,j \rangle\rangle} (e^{i\phi_{ij}} a_i^\dagger a_j + \text{H.c.}), \\ H_{\text{NN}} &= V \sum_{\langle i,j \rangle} n_i n_j, \end{aligned} \quad (1)$$

where a_i^\dagger (a_i) is the hard-core boson creation (annihilation) operator at site i and $n_i = a_i^\dagger a_i$ is the corresponding number operator. In this Hamiltonian, J_1 and J_2 are the NN and NNN hopping amplitudes, respectively, and $V (> 0)$ is the parameter of the NN repulsion, which may be produced by the dipole-dipole interaction¹⁰. The NNN hopping term is complex $J_2 e^{i\phi_{ij}}$ with the phase $\phi_{ij} = \pm\phi$ (th sign \pm will be specified in the later discussion), which is experimentally feasible by the time-periodic driving of the honeycomb optical lattice.

Reflecting the hard-core nature, the physical Hilbert space consists of states in which the particle number at each site is less than unity. In order to incorporate the local constraint faithfully, we employ the following slave-particle representation,

$$a_i = h_i^\dagger b_i, \quad (2)$$

with the constraint,

$$(b_i^\dagger b_i + h_i^\dagger h_i - 1)|\text{Phys}\rangle = 0, \quad (3)$$

where b_i^\dagger (b_i) and h_i^\dagger (h_i) are the boson and hole operator at site i , respectively. $|\text{Phys}\rangle$ denotes the physical

subspace of the slave particles corresponding to the hard-core boson. From Eqs.(2) and (3), it is not difficult to show that the operators a_i and a_i^\dagger on the same site satisfy the anti-commutation relation such as $\{a_i, a_i^\dagger\} = 1$ and $\{a_i, a_i\} = \{a_i^\dagger, a_i^\dagger\} = 0$, whereas the usual bosonic commutation relations such as $[a_i, a_j^\dagger] = 0$, etc., for $i \neq j$. For example in the slave-particle representation,

$$\begin{aligned} (a_i a_i^\dagger + a_i^\dagger a_i) b_i^\dagger |0\rangle &= (h_i^\dagger b_i b_i^\dagger h_i + b_i^\dagger h_i h_i^\dagger b_i) b_i^\dagger |0\rangle \\ &= b_i^\dagger |0\rangle, \end{aligned}$$

where we have used the ordinary bosonic commutation relations of the slave particles b_i and h_i and the constraint Eq.(3). The standard path integral for the Bose particles *with the faithful local constraint* guarantees the above hard-core commutation relations.

In most of the later discussions, we consider the half-filling case, which corresponds to the case $\langle \sum_i S_i^z \rangle = 0$ in the spin system.

Note that the system described by the Hamiltonian [Eq.(1)] is closely related to a $s = 1/2$ AF spin model on the honeycomb lattice by the correspondence such as $a_i^\dagger \rightarrow S_i^+$, $a_i \rightarrow S_i^-$, $(n_i - \frac{1}{2}) \rightarrow S_i^z$, $H_{\text{BH}} \rightarrow H^S$,

$$\begin{aligned} H^S &= H_0^S + H_{\text{NN}}^S + H^Z, \\ H_0^S &= J_1 \sum_{\langle i,j \rangle} (S_i^+ S_j^- + \text{H.c.}) \\ &\quad + J_2 \sum_{\langle\langle i,j \rangle\rangle} (e^{i\phi_{ij}} S_i^+ S_j^- + \text{H.c.}), \end{aligned} \quad (4)$$

$$H_{\text{NN}}^S = V \sum_{\langle i,j \rangle} S_i^z S_j^z, \quad H^Z = \frac{3}{2} V \sum_i S_i^z, \quad (5)$$

where S_i^\pm are the operators that flip a spin at site i . J_1 and J_2 correspond to the NN and NNN spin exchange couplings. For $J_1, J_2 > 0$, the NNN coupling generates the frustration whose strength is controlled by the parameter ϕ for $0 \leq \phi < \pi$. The chemical potential is introduced in the boson system in order to cancel the Zeeman term H^Z although we do not show it explicitly.

In our previous numerical studies^{7,8,11}, the results of the MC simulations show that density fluctuation at each lattice site is not large even in the spatially inhomogeneous states like a density-wave state. From this observation, we expect that the following term appears,

$$H_1 = V_0 \sum_i \left((b_i^\dagger b_i - \rho_{bi})^2 + (h_i^\dagger h_i - \rho_{hi})^2 \right), \quad (6)$$

where ρ_{bi} (ρ_{hi}) is the parameter that controls the mean density of boson (hole) at site i , and $V_0 (> 0)$ controls its fluctuation from the mean value ρ_{bi} (ρ_{hi}). We impose the local constraint such as $\rho_{bi} + \rho_{hi} = 1$ in the MC simulation. It is expected that the hopping terms in H_{BH} (i.e., H_0) enhance homogeneous configurations, and induces terms such as H_1 . In Ref.¹¹, we discussed how H_1 [Eq. (6)] appears from the hopping terms in the Hamiltonian and the rough estimation of the parameter V_0 gives

$V_0 \sim J_1/\rho_{bi}$. However, the precise value of V_0 depends on the dynamics of the phase degrees of freedom of the slave particles¹¹. Then in the present work, we put typical values for V_0 and verify the stability of the numerical results¹². We explicitly add this term to the Hamiltonian and consider the system $H_{\mathcal{T}} = H_{\text{BH}} + H_1$. The existence of H_1 is very useful for study of the quantum many-particle systems by the path-integral MC simulation.

The model $H_{\mathcal{T}}$ is studied by the path-integral methods¹¹. To this end, we introduce the coherent states for the slave particles as follows,

$$\begin{aligned} b_i|\varphi_{bi}\rangle &= \varphi_{bi}|\varphi_{bi}\rangle = \sqrt{\rho_{bi} + \delta\rho_{bi}} e^{i\theta_{bi}}|\varphi_{bi}\rangle, \\ h_i|\varphi_{hi}\rangle &= \varphi_{hi}|\varphi_{hi}\rangle = \sqrt{\rho_{hi} + \delta\rho_{hi}} e^{i\theta_{hi}}|\varphi_{hi}\rangle, \end{aligned} \quad (7)$$

where $\delta\rho_{bi}$ ($\delta\rho_{hi}$) is the quantum fluctuation of the density around the mean value ρ_{bi} (ρ_{hi}) at site i and θ_{bi} (θ_{hi}) is the phase degrees of freedom. In the path-integral representation of the partition function Z , the action contains the imaginary terms like $\int d\tau \bar{\varphi}_i(\tau) \partial_{\tau} \varphi_i(\tau)$, where $\bar{\varphi}_i$ stands for the coherent field of b_i^{\dagger} (h_i^{\dagger}) and τ is the imaginary time, i.e.,

$$\begin{aligned} Z &= \int [D\varphi_b D\varphi_h] \exp \left[- \int d\tau \left(\bar{\varphi}_{bi}(\tau) \partial_{\tau} \varphi_{bi}(\tau) \right. \right. \\ &\quad \left. \left. + \bar{\varphi}_{hi}(\tau) \partial_{\tau} \varphi_{hi}(\tau) + H_{\mathcal{T}} \right) \right], \end{aligned} \quad (8)$$

where $H_{\mathcal{T}}$ is expressed by the slave particles and the above path integral is calculated under the constraint Eq.(3). For the existence H_1 , we separate the path-integral variables b_i and h_i as Eq.(7) and we integrate out the fluctuations $\delta\rho_{bi}$ and $\delta\rho_{hi}$. However, there exists the constraint such as $\delta\rho_{bi} + \delta\rho_{hi} = 0$ on performing the path-integral over $\delta\rho_{bi}$ and $\delta\rho_{hi}$. This constraint can be readily incorporated by using a Lagrange multiplier λ_i ,

$$\prod_{\tau} \delta(\delta\rho_{bi} + \delta\rho_{hi}) = \int d\lambda_i e^{i \int d\tau (\delta\rho_{bi} + \delta\rho_{hi}) \lambda_i}. \quad (9)$$

The variables $\delta\rho_{bi}$ and $\delta\rho_{hi}$ also appear in H_0 and H_{NN} , but we ignore them. On integration, linear terms of $\delta\rho_{bi}$ and $\delta\rho_{hi}$ in H_{BH} are absent as we require the minimal energy condition to determine the mean values of ρ_{bi} and ρ_{hi} . Please see the later discussion. As we remarked in the above, quadratic terms of $\delta\rho_{bi}$ and $\delta\rho_{hi}$ in H_0 are partly incorporated in H_1 , although the precise estimation of V_0 is lacking. For the case with $V > 0$, which is discussed in Sec. VI, the quadratic terms of the density fluctuations in the repulsion term generate spatially nonlocal terms of $\partial_{\tau} \theta_{bi}$ and $\partial_{\tau} \theta_{hi}$. We shall ignore these terms in the practical calculation and therefore we may underestimate the phase-ordered states. With this approximation, we have,

$$\begin{aligned} &\int d\lambda_i d\delta\rho_{bi} d\delta\rho_{hi} \exp \left[\int d\tau \left(-V_0 (\delta\rho_{bi}^2 + \delta\rho_{hi}^2) \right. \right. \\ &\quad \left. \left. + i\delta\rho_{bi} (\partial_{\tau} \theta_{bi} + \lambda_i) + i\delta\rho_{hi} (\partial_{\tau} \theta_{hi} + \lambda_i) \right) \right] \\ &= \int d\lambda_i e^{-\frac{1}{4V_0} \int d\tau ((\partial_{\tau} \theta_{bi} + \lambda_i)^2 + (\partial_{\tau} \theta_{hi} + \lambda_i)^2)}, \end{aligned} \quad (10)$$

where we have ignored the terms like $\int d\tau \partial_{\tau} \theta_{bi}$ ($\int d\tau \partial_{\tau} \theta_{hi}$) by the periodic boundary condition for the imaginary time. The resultant quantity on the right-hand side (RHS) of Eq.(10) is positive-definite, and therefore the numerical study by the MC simulation can be performed without any difficulties. It should be remarked that the Lagrange multiplier λ_i in Eq.(10) behaves as a gauge field, i.e., the RHS of Eq.(10) is invariant under the following ‘‘gauge transformation’’, $\theta_{bi} \rightarrow \theta_{bi} + \alpha_i$, $\theta_{hi} \rightarrow \theta_{hi} + \alpha_i$, $\lambda_i \rightarrow \lambda_i - \partial_{\tau} \alpha_i$. It is easily shown that all physical quantities are invariant under the above gauge transformation. Finally, we have an effective action S , with which the partition function is given as follows,

$$\begin{aligned} Z &= \int [d\theta_{bi}] [d\theta_{hi}] e^{-S}, \quad (11) \\ S &= \int d\tau \left(\sum_i \frac{1}{4V_0} ((\partial_{\tau} \theta_{bi} + \lambda_i)^2 + (\partial_{\tau} \theta_{hi} + \lambda_i)^2) \right. \\ &\quad \left. + J_1 \sum_{\langle i,j \rangle} \sqrt{\rho_{bi} \rho_{hi} \rho_{bj} \rho_{hj}} \cos(\theta_i - \theta_j) \right. \\ &\quad \left. + J_2 \sum_{\langle\langle i,j \rangle\rangle} \sqrt{\rho_{bi} \rho_{hi} \rho_{bj} \rho_{hj}} \cos(\theta_i - \theta_j - \phi_{ij}) \right) \\ &\quad + V \sum_{\langle i,j \rangle} \rho_{bi} \rho_{bj}, \end{aligned} \quad (12)$$

where $\theta_i \equiv \theta_{bi} - \theta_{hi}$. As the slave particles always appear in the composite $b_i h_i^{\dagger}$, the symmetric degrees of freedom $\theta_i \equiv \theta_{bi} + \theta_{hi}$ decouple, except the first kinetic term of the action S including $\partial_{\tau} \theta_{bi}$ and $\partial_{\tau} \theta_{hi}$.

III. EXTENDED MONTE-CARLO SIMULATION

In the previous section, the effective action S was derived. For the MC simulation, we introduce a lattice in the imaginary-time τ -direction with the lattice spacing $\Delta\tau$. In order to impose the local constraint Eq.(3), $\rho_{bi} + \rho_{hi} = 1$, we parameterize ρ_{bi} and ρ_{hi} as $\rho_{bi,\ell} = \sin^2(\chi_{i,\ell})$, $\rho_{hi,\ell} = \cos^2(\chi_{i,\ell})$, where $\chi_{i,\ell}$ is angle variable and (i, ℓ) denotes site in a stacked honeycomb lattice (ℓ is imaginary-time index). Thus, the effective action S becomes a kind of 3D XY model defined on the space-time lattice, whereas its coefficients depend on the variational parameters $\{(\rho_{bi,\ell}, \rho_{hi,\ell})\}$. The lattice action and partition function of the lattice model are given as follows:

$$\begin{aligned} Z_{\text{L}} &= \int \prod_{\ell=0}^{N_{\tau}-1} \prod_i [d\chi_{i,\ell} d\theta_{bi,\ell} d\theta_{hi,\ell} d\lambda_{i,\ell}] e^{-S_{\text{L}}}, \quad (13) \\ S_{\text{L}} &= \sum_{\ell=0}^{N_{\tau}-1} \left[\sum_i -\frac{1}{2V_0 \tau \Delta\tau} \cos(\theta_{bi,\ell+1} - \theta_{bi,\ell} + \lambda_{i,\ell}) \right. \\ &\quad \left. + \sum_i -\frac{1}{2V_0 \tau \Delta\tau} \cos(\theta_{hi,\ell+1} - \theta_{hi,\ell} + \lambda_{i,\ell}) \right] \end{aligned}$$

$$\begin{aligned}
& + \frac{1}{2} J_1 \Delta\tau \sum_{\langle i,j \rangle} \sin(2\chi_{i,\ell}) \sin(2\chi_{j,\ell}) \cos(\theta_{i,\ell} - \theta_{j,\ell}) \\
& + \frac{1}{2} J_2 \Delta\tau \sum_{\langle i,j \rangle} \sin(2\chi_{i,\ell}) \sin(2\chi_{j,\ell}) \cos(\theta_{i,\ell} - \theta_{j,\ell} - \phi_{ij}) \\
& + V \Delta\tau \sum_{\langle i,j \rangle} \sin^2(\chi_{i,\ell}) \sin^2(\chi_{j,\ell}) \\
& - \sum_i \ln(\sin(2\chi_{i,\ell})) \Big], \tag{14}
\end{aligned}$$

where N_τ is the linear system size of the τ -direction and is related to the temperature (T) as $N_\tau \Delta\tau = 1/(k_B T)$, and all variables are periodic in the τ -direction. It should be remarked here that $\Delta\tau$ is nothing but the inverse temperature and by changing $\Delta\tau$, T is controlled. The last term in Eq.(14) comes from the change of variables from $(\rho_{bi,\ell}, \rho_{hi,\ell})$ to $\chi_{i,\ell}$. As we explained above, as the physical (original) particle a_i is the composite of b_i and h_i^\dagger [Eq.(2)], the effective model is invariant under a local gauge transformation such as $(\theta_{bi,\ell}, \theta_{hi,\ell}, \lambda_{i,\ell}) \rightarrow (\theta_{bi,\ell} + \alpha_{i,\ell}, \theta_{hi,\ell} + \alpha_{i,\ell}, \lambda_{i,\ell} - \alpha_{i,\ell+1} + \alpha_{i,\ell})$ where $\alpha_{i,\ell}$ is an arbitrary parameter ($\alpha_{i,N_\tau+1} = \alpha_{i,1}$). It seems that the ‘‘gauge field’’ $\lambda_{i,\ell}$ can be eliminated by the gauge fixing, but this is not the case. After the gauge fixing, there remains one degree of freedom per site i , i.e., so-called zero mode, $\sum_{\ell=1}^{N_\tau} \lambda_{i,\ell}$. In the MC simulation, we remain the gauge field $\lambda_{i,\ell=1}$ as MC variables whereas we put the others $\lambda_{i,\ell \neq 1} = 0$.

The effective action in the path-integral formalism includes both the variational parameters $\{(\rho_{bi,\ell}, \rho_{hi,\ell})\} \rightarrow \{\chi_{i,\ell}\}$ and the dynamical phase variables, $\{\theta_{bi}\}$ and $\{\theta_{hi}\}$. We determine the variational variables $\{(\rho_{bi,\ell}, \rho_{hi,\ell})\}$ by the minimum-energy condition by using MC methods. In the practical calculation of Eq.(14), we treat $\{(\rho_{bi,\ell}, \rho_{hi,\ell})\}$ as slow variables in the MC local-update, keeping the mean densities constant. As the effective action S_L in Eq.(14) is real and bounded from below, there exist no difficulties in performing MC simulations. In the following sections, we shall show the numerical results and discuss the physical meaning of them.

IV. NUMERICAL RESULTS FOR $V = \phi = 0$ CASE

In this section and subsequent sections, we shall show the results obtained by the MC simulation. The effective model is defined by Eq.(14) and we employ the standard Metropolis algorithm with the local updates¹³. For the local update of the phase degrees of freedom θ , random variables $\Delta\theta$ used for generating a candidate of a new variable $\theta_{new} = \theta_{old} + \Delta\theta$ was chosen in the range $|\Delta\theta| \leq \pi/6$. Furthermore in this study, the local average densities are also variational parameters and are parameterized by the angle variables $\{\chi_{i,\ell}\}$. Since the local average densities are slow variables, the range of random variables $\Delta\chi_{i,\ell}$ are restricted as $|\Delta\chi_{i,\ell}| \leq \pi/60$. The typ-

ical sweep for the thermalization is 100 000 and for the measurement is $(40\,000) \times (10\text{ samples})$. The typical acceptance ratio is 40%~50%, and errors were estimated from 10 samples by the jackknife method¹⁴.

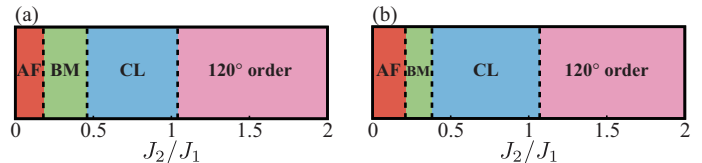


FIG. 1. (Color online) Phase diagrams of the Bose-Hubbard model on the honeycomb lattice with $V = \phi = 0$. (a) $V_0 = 5$, (b) $V_0 = 0.5$. There are four phases, antiferromagnetic (AF), Bose metal (BM), collinear (CL) and 120° -order state. Lattice size is small, $(L_x, L_y) = (3, 4)$.

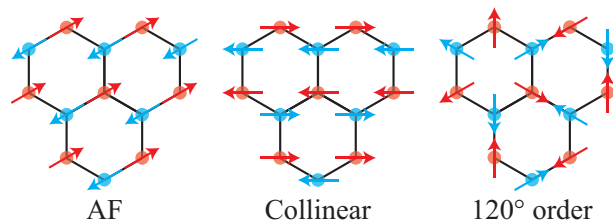


FIG. 2. (Color online) Spin (phase θ_i) configurations of the three ordered states, antiferromagnetic (AF), collinear (CL) and 120° -order phase in the phase diagram in Fig. 1.

A. Low-temperature phase diagrams

We first show the phase diagrams as a function of the dimensionless parameter J_2/J_1 for the case of $V = \phi = 0$ ¹⁵. In the practical calculation, we put $J_1 = 10$ and $\Delta\tau = 1$. See Fig. 1 for the phase diagrams for $V_0 = 5$ and $V_0 = 0.5$. For the case of the system size $(L_x, L_y) = (3, 4)$ and $N_\tau = 8$, there are four phases, i.e., AF, BM, collinear (CL), and 120° -order state. There exist no qualitative differences between the phase diagrams of the $V_0 = 5$ and $V_0 = 0.5$ cases.

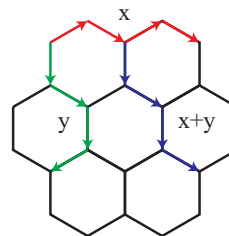


FIG. 3. (Color online) x , y and $x + y$ -directions on the honeycomb lattice.

To clarify the phase diagrams, we calculated various physical quantities. Phase boundaries were determined by calculating the “internal energy” E and the “specific heat” C , which are defined as

$$E = \frac{\langle S_L \rangle}{N}, \quad C = \frac{\langle (S_L - \langle S_L \rangle)^2 \rangle}{N}, \quad (15)$$

where $N = N_x N_y$ is the total number of sites in the stacked honeycomb lattice and we employ the periodic boundary condition. We also calculate correlation functions on the honeycomb lattice in the x , y , and $x + y$ directions (see Fig. 3), which are defined as follows,

$$G_{x(y)(x+y)}(r) = \frac{1}{N_{2D}} \sum_i \langle \cos(\theta_{i+r} - \theta_i) \rangle, \quad (16)$$

where the site $i + r$ denotes the sites with distance r from the site i in the x , y and $x + y$ directions in the honeycomb lattice, respectively.

For the phases except the BM, the order parameter, $\langle a_i \rangle$, has a coherent phase, as shown by the calculated correlation functions. Spin (phase of $\langle a_i \rangle = \theta_i$) configurations for the phases in the phase diagram in Fig. 1 are depicted in Fig. 2. From Fig. 2, we identified the AF, CL, and 120° -order phase. As we show shortly for a larger system, the BM has only a short-range correlation of $\langle a_i \rangle$.

There are results of the exact diagonalization for the system with the size $(L_x, L_y) = (3, 4)$ ($N_{2D} = 24$). Qualitatively the same phase diagram with those in Fig. 1 was obtained. Critical values of J_2/J_1 of the exact diagonalization at which the phase transitions take place are very close to those obtained in this work, in particular, the result with $V_0 = 0.5$.

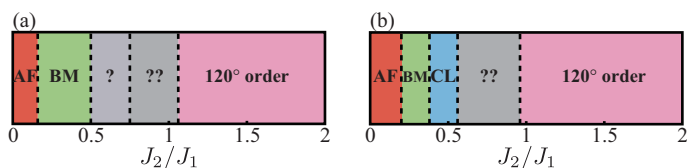


FIG. 4. (Color online) Phase diagrams of the Bose-Hubbard model on the honeycomb lattice with $V = \phi = 0$. (a) $V_0 = 5$, (b) $V_0 = 0.5$. There are unidentified phases besides antiferromagnetic (AF), Bose metal (BM), colinear (CL) and phase with the 120° order. Lattice size, $(L_x, L_y) = (6, 6)$.

As the system has the strong frustrations for the case of $\phi = 0$, it is important to see if the phase diagram depends on the system size. In order to see this, we studied the system with $(L_x, L_y) = (6, 6)$. No exact diagonalization results are available for this system size. Obtained phase diagrams are shown in Fig. 4. Compared with the previous result of $(L_x, L_y) = (3, 4)$, there are additional phases whose spin (i.e., phase θ_i) configuration cannot be depicted globally.

Calculations of the specific heat used to obtain the phase diagrams in Figs. 1 and 4 are shown in Fig. 5. As

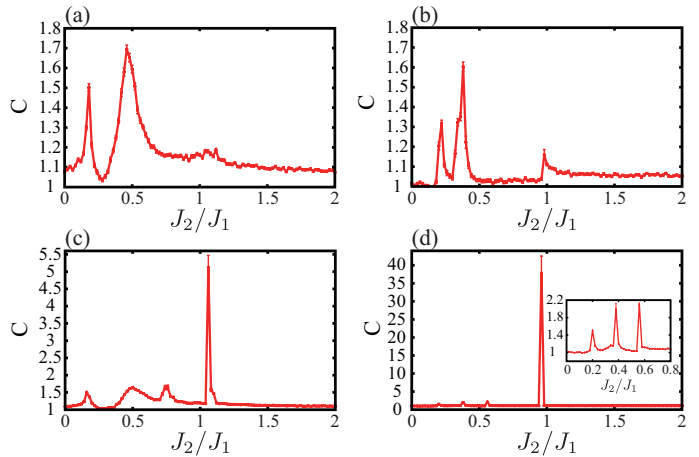


FIG. 5. (Color online) Specific heat C for the case of $V = \phi = 0$. (a) $(L_x, L_y) = (3, 4)$ and $V_0 = 5$, (b) $(L_x, L_y) = (3, 4)$ and $V_0 = 0.5$, (c) $(L_x, L_y) = (6, 6)$ and $V_0 = 5$, (d) $(L_x, L_y) = (6, 6)$ and $V_0 = 0.5$. Sharp peaks in the system with $(L_x, L_y) = (6, 6)$ indicate that the transition is of first order. This is verified by the measurement of the internal energy E .

the system size is getting larger, not only the peaks of C get sharper but also other peaks appear. Compared with systems without frustrations studied in previous works, the specific heat C has very strong system-size dependence in the present case.

To identify the phases, we calculated the correlation functions in Eq.(16). The results are shown in Fig. 6. We verified that all the numerical results are quite stable even for the unidentified phases in the phase diagram in Fig. 4. Phases (a), (c) and (d) are the AF, CL and 120° phases, respectively, and the phase (b) is the BM without long-range correlations. The calculation of the specific heat indicates the existence of the phases (e) and (f). The phase (e) and (f) have rather clear spin correlations as shown in Fig. 6, but it is difficult to depict global configurations of the phase of $\langle a_i \rangle$.

It is sometimes useful to see the particle density in the wave-vector space, which is defined as,

$$\begin{aligned} n(\mathbf{k}) &= \langle a^\dagger(\mathbf{k})a(\mathbf{k}) \rangle \\ &= \sum_{i,j} e^{-\mathbf{k} \cdot (\mathbf{r}_i - \mathbf{r}_j)} \langle a_i^\dagger a_j \rangle, \end{aligned} \quad (17)$$

where \mathbf{r}_i and \mathbf{r}_j are lattice vectors corresponding to sites i and j of the honeycomb lattice, respectively. We show the calculations of $n(\mathbf{k})$ in Fig. 7. In the AF, CL and 120° -order phases, particles condensate at some specific momenta consistent with the correlation function, whereas in the BM no clear pattern can be seen. On the other hand for the phases (e) and (f), the particle density has moderate but rather clear peaks at three spots although their locations are incommensurate with the Brillouin zone.

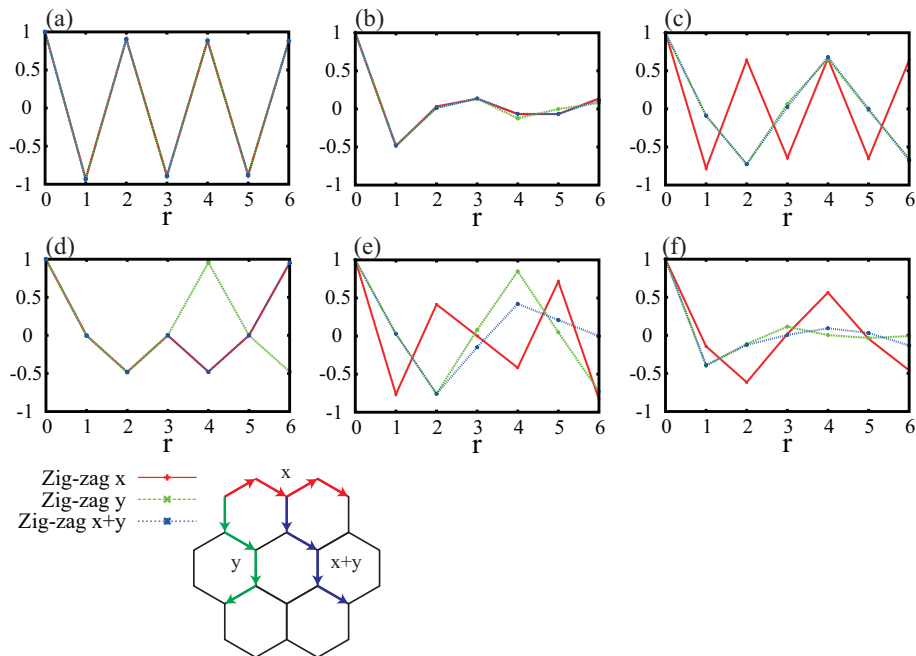


FIG. 6. (Color online) Correlation functions in Eq.(16) for the phases in Fig. 4. (a) AF, (b) BM, (c) CL, (d) 120° -order state, and (e) and (f) are phases whose existence is indicated by the calculation of the specific heat.

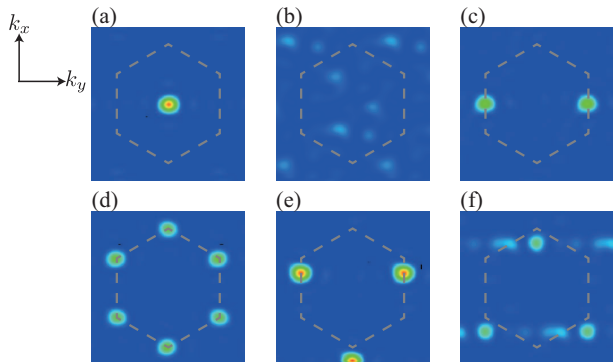


FIG. 7. (Color online) Density distribution in the momentum space $n(\mathbf{k})$ defined by Eq.(17) for the phases in Fig. 4. (a) AF, (b) BM, (c) CL, (d) 120° -order state, and (e) and (f) are phases whose existence is indicated by the calculation of the specific heat. The dotted line denotes the boundary of the Brillouin zone.

It is quite interesting to see if the BM is gapless or gapful. To study this problem, we notice that a change of the parameter $\Delta\tau$ corresponds to a change of the system temperature T . From this fact, we can measure the T -dependence of the specific heat C . Furthermore, if signals of phase transition do not appear as T is increased, we conclude that the BM has no LROs.

B. Finite-temperature phase transitions for $V = \phi = 0$ case

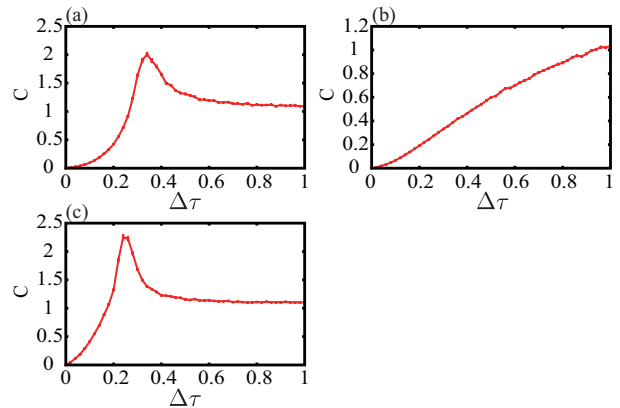


FIG. 8. (Color online) Finite- T phase transitions for the AF [(a)], BM [(b)], and 120° -order state [(c)] phases, respectively. The thermal specific heat C_T exhibits a sharp peak for the AF and the 120° -order phase, whereas there is no signal of the phase transition for the BM. This result indicates that the BM does not have any long-range orders. C_T for the AF and the 120° -order phase approaches to a constant close to unity at low T limit. $V_0 = 5$.

In this section, we shall study finite- T effects on the phases observed in the previous subsection¹⁶. In particular, it is interesting to see if a phase transition takes place or not in the BM, i.e., the existence of a finite- T phase

transition means that the BM phase has a certain order at low (vanishing) T , or vice versa. On the other hand, we expect that a finite- T phase transition takes place at a certain critical T_c for the AF and 120° -order states.

As we explained previously, $N_\tau \Delta\tau = 1/(k_B T)$, and therefore a decrease of $\Delta\tau$ corresponds to an increase of T . The finite- T system is described by the effective action S_L in Eq.(14) with $\Delta\tau < 1$. It should be remarked here that the present numerical parameters such as $J_1 \Delta\tau = 10$ and $N_\tau = 8$ corresponds to $k_B T = J_1/80$, which means a very low T . We study the system with the lattice size $(L_x, L_y) = (6, 6)$, and focus on the AF, BM, and 120° -order state.

Numerical result of *the thermal specific heat* C_T is given in Fig. 8, where the thermal specific heat C_T is defined as follows,

$$\begin{aligned}
 C_T &= \frac{1}{N_{2D}} \left[\langle (H_\beta)^2 \rangle - \langle H_\beta \rangle^2 \right], \\
 H_\beta &\equiv \sum_{\ell=0}^{N_\tau-1} \left[\frac{1}{2} J_1 \Delta\tau \sum_{\langle i,j \rangle} \sin(2\chi_{i,\ell}) \sin(2\chi_{j,\ell}) \cos(\theta_{i,\ell} - \theta_{j,\ell}) \right. \\
 &\quad + \frac{1}{2} J_2 \Delta\tau \sum_{\langle i,j \rangle} \sin(2\chi_{i,\ell}) \sin(2\chi_{j,\ell}) \cos(\theta_{i,\ell} - \theta_{j,\ell}) \\
 &\quad + V \Delta\tau \sum_{\langle i,j \rangle} \sin^2(\chi_{i,\ell}) \sin^2(\chi_{j,\ell}) \\
 &\quad \left. - \sum_i \ln(\sin(2\chi_{i,\ell})) \right]. \tag{18}
 \end{aligned}$$

It is obvious that C_T exhibits a sharp peak for the AF and 120° -order state, whereas no peaks for the BM. This result means that the BM does not have any long-range orders. We verified that the orders of the AF and 120° -order state are destroyed at T_c identified by C_T .

At low $T < T_c$ ($\Delta\tau > \Delta\tau_c$), C_T for the AF and 120° -order state has a constant value close to unity. This behavior indicates that a stable quasi-excitation exists that is nothing but a Nambu-Goldstone mode appearing as a result of the spontaneous U(1) symmetry breaking. On the other hand for the BM, C_T increases as T decreases. This implies that excitations in the BM are *not* simple gapless quasi-particles and a strongly-correlated (strongly-frustrated) state forms in the BM.

V. PHASE DIAGRAM IN $(J_2/J_1-\phi)$ PLANE

In this section, we study the phase diagram of the BHHM with nonvanishing ϕ (the phase of the NN hopping), whereas we keep the NN repulsion $V = 0$. As the case of $\phi = 0$ is the most frustrated system, it is expected that turning on ϕ makes the system more tractable and stabilizes the ground-state. There are two possible ways to introduce the phase ϕ_{ij} in the NN hopping as depicted in Fig. 9, one of which is called original Haldane model and the other is called modified Haldane model¹⁷. As

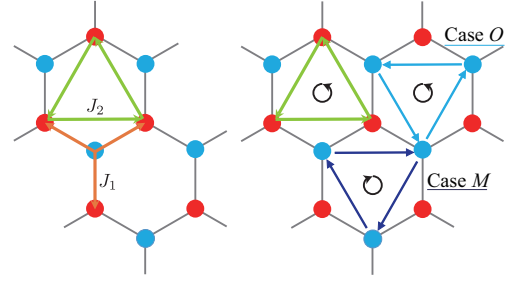


FIG. 9. (Color online) Hopping terms in the BHHM. The NNN hopping amplitudes with an arrow are $J_2 e^{i\phi}$. Case O (M) refers to the original (modified) model.

we show, these two models can have different phase diagrams as in the ferromagnetic NN coupling cases studied in the previous paper⁸.

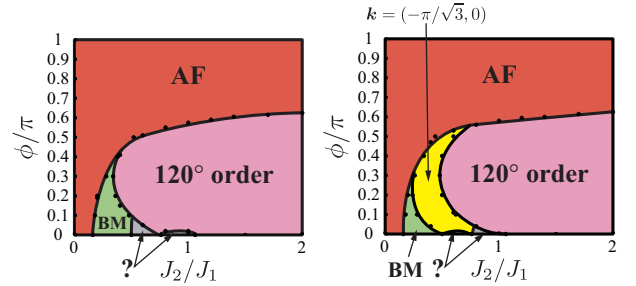


FIG. 10. (Color online) Phase diagrams of the original (left) and modified (right) BHHMs. Finite ϕ makes the system less frustrated, and clear phase boundaries are obtained. $V_0 = 5$ and the system size $(L_x, L_y) = (6, 6)$.

By using the same extended MC simulations, we obtained the phase diagrams of the original and modified BHHMs as in Fig. 10. Even for very small ϕ , the phase boundaries are obtained rather clearly. Calculations of the internal energy and specific heat indicate that the phase transition AF \leftrightarrow 120° -order state is of first order, whereas both AF \leftrightarrow BM and $120^\circ \leftrightarrow$ BM transitions are continuous ones. This result again implies that the BM does not have any long-range orders. In the experimental set up to realize the Bose-Haldane model on the honeycomb lattice, it is expected that the value of ϕ can be a controllable parameter. Careful study on the phase diagram by experiments may shed light on the physical properties of the phases with $\phi = 0$ and related AF magnets on the honeycomb lattice.

In the phase diagram of the modified BHHM, there appears another ordered phase that we call $\mathbf{k} = (-\pi/\sqrt{3}, 0)$ phase. Details are shown in Fig. 11. Phase closely related to this was recently observed for a frustrated Heisenberg model on the honeycomb lattice¹⁸. In the present case, the reduction of the frustration by a finite ϕ makes this phase stable for a rather large region of the phase diagram. Angles between the NN spins and also NNN spins

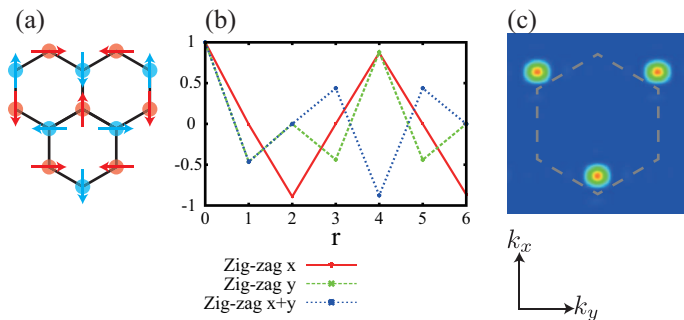


FIG. 11. (Color online) Properties of the $\mathbf{k} = (-\pi/\sqrt{3}, 0)$ phase. (a) spin configuration, (b) correlation function, and (c) density distribution in the momentum space.

are either $\pi/2$ or π . The particle distribution functions $n(\mathbf{k})$ in Fig. 7(e) and Fig. 11(c) indicate that the phase in Fig. 7(e) and the $\mathbf{k} = (-\pi/\sqrt{3}, 0)$ phase have some similarity although there exists a phase boundary between them as shown in the phase diagram of Fig. 10.

VI. PHASE DIAGRAM WITH NN INTERACTION

In this section, we study the system in which the NN interaction H_{NN} in Eq. (1) exists¹⁹. As mentioned previously, this term corresponds to the AF-spin coupling in the z -component such as $V \sum_{\langle i,j \rangle} S_i^z S_j^z$. The previous study on some related models shows that the inclusion of the NN interaction H_{NN} makes the system stable as the frustration in the XY component is weakened by the existence of this term⁸. For sufficiently large V , it is expected that the charge-density order appears, which corresponds to the AF order in the z -component of spin.

We investigated the system with $\phi = 0$ and $V > 0$ by the extended MC simulations as before and obtained the phase diagrams shown in Fig. 12. The system is at half filling with $\mu/V = 1.5$, i.e., $\langle \sum_i S_i^z \rangle = 0$, and we put $J_1 = 10$ and $\Delta\tau = 1$ as before. For small J_2 and ϕ , the BM still exists as in the pure XY case. As V is getting large, the state with the charge-density wave (CDW) forms. The phase transition $\text{AF} \leftrightarrow \text{CDW}$ and $120^\circ\text{-order state} \leftrightarrow \text{CDW}$ are both first-order phase transitions, whereas the transition between the BM and CDW is a continuous one. The internal energy E and specific heat C are shown in Fig. 13. At the $\text{AF} \leftrightarrow \text{CDW}$ phase transition, E exhibits a step-wise behavior although hysteresis is not observed. At the critical point, C has a very large and steep peak. On the other hand, C shows a step-wise behavior at the $\text{BM} \leftrightarrow \text{CDW}$ transition. Although C has no sharp peak, this anomalous behavior of C indicates that a second-order phase transition or a crossover takes place between the BM and CDW. Again, this result indicates that there are no LROs in the BM.

For the AF XY spin model on the honeycomb lattice

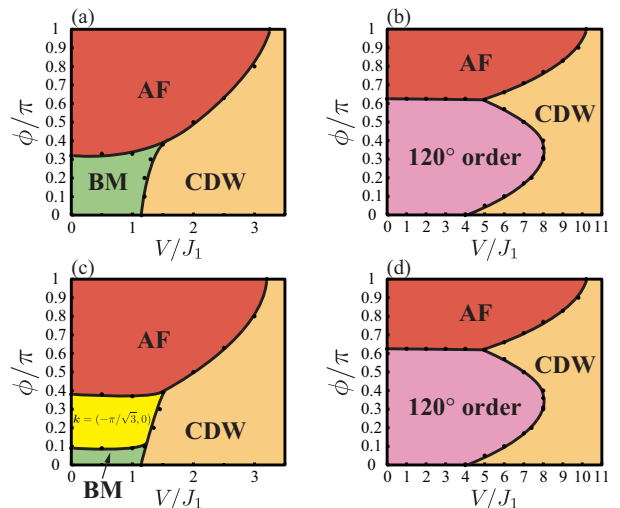


FIG. 12. (Color online) Phase diagrams of the BHHM with the NN interaction $V > 0$. $J_1 = 10$ and $V_0 = 5$. (a) original BHHM with $J_2 = 3$, (b) original BHHM with $J_2 = 20$, (c) modified BHHM with $J_2 = 3$, (d) modified BHHM with $J_2 = 20$. For $J_2 = 20$, the phase diagrams of the original and modified BHHM are almost the same as the NNN hopping dominates over the NN hopping. The system is at half filling with $\mu/V = 1.5$.

of the cylinder geometry, the density-matrix renormalization group study showed that in the intermediate parameter region of J_2/J_1 , unexpected AF order in the z -direction forms²⁰. In the present study on the hard-core BHHM, the above parameter region corresponds to the BM in Fig. 12 (a) with $V, \phi \sim 0$. We measured the density correlation in the BM near the phase boundary to the CDW and found a short-range correlation as it is expected. Then, it is interesting to study the BHHM on the honeycomb lattice of the cylinder geometry and to see if such a density order persists in the deep BM region. This problem will be studied and results will be published in the near future.

VII. CONCLUSION

In this paper, we studied the hard-core BHHM in which the frustration caused by the NN and NNN hoppings exists. Strength of the frustration is controlled by the phase ϕ of the NNN hopping. This model is closely related with the spin-1/2 AF magnets and it is expected that a state without any long-range orders exists in a moderate parameter region of the phase diagram.

We first considered the case with $\phi = 0$ and the vanishing NN repulsion, i.e., the most frustrated case. The extended MC simulation shows that the AF, CL and $120^\circ\text{-order state}$ form as the NNN amplitude increases, while there appears the state that we call the BM between the AF and CL. Correlation functions and the or-

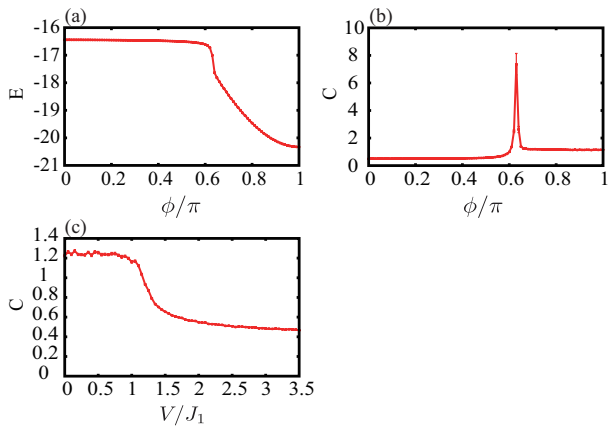


FIG. 13. (Color online) Internal energy E and specific heat C measured in the phases in Fig. 12. $V_0 = 5$. (a) E as a function of ϕ in the original BHHM with $J_1 = 10$, $J_2 = 3$ and $V = 25$, (b) C as a function of ϕ in the original BHHM with $J_1 = 10$, $J_2 = 3$ and $V = 25$ (c) C as a function of V/J_1 of the original BHHM with $J_2 = 3.0$. Phase transition between the AF and CDW is of first order, and that between the BM and CDW is of second order. The system is at half filling with $\mu/V = 1.5$, where μ is the chemical potential of the BHHM.

der of the phase transition indicate that the BM has no LROs. We also studied the finite- T phase diagram and found that no transitions take place from the BM as T is increased. Therefore we concluded that the BM is a featureless state. On the other hand, all the above mentioned ordered states transit to disordered states through the second-order phase transitions.

Results of the MC simulations show a strong system-size dependence of the phase diagram. The results for the $(L_x, L_y) = (3, 4)$ system (a small system) are in good agreement with the results obtained by the exact diagonalization for the same system size⁹. On the other hand, the larger system with $(L_x, L_y) = (6, 6)$ has a slightly

different phase diagram in which additional unidentified phases appear. Investigation of these states is a future problem. [No results of the exact diagonalization are available for the $(L_x, L_y) = (6, 6)$ case.]

Next we studied the phase diagram in the $(J_2/J_1 - \phi)$ plane. There are two types of the BHHM named the original and modified BHHMs, respectively. As increasing the value of ϕ , stable states and phase boundaries appear. Besides the ordered states in the $\phi = 0$ case, there appear another ordered state that we call $\mathbf{k} = (-\pi/\sqrt{3}, 0)$ state. Finally, we examined the effect of the NN repulsion. Inclusion of the NN repulsion, which corresponds to the AF coupling $V \sum_{\langle i,j \rangle} S_i^z S_j^z$, stabilizes the frustration. As V is increased, the CDW forms that corresponds to the Ising-type AF configuration in the z -component.

We obtained the “multi-dimensional phase diagram” in this work. The result suggests feasible experiments that quantum simulate the BHHM with cold atomic gases on the optical lattice. We expect that these quantum simulation clarifies the physical nature of the BM as well as the unidentified states observed in this study. This must shed light on the physical nature of the spin liquid in the AF magnets on the honeycomb lattice.

Finally, recently some related spin and boson models were analytically studied by using the Chern-Simon gauge theory. There, dynamical variables are described by using fermions and various phase diagrams were obtained²¹. It is interesting and also important to extend the present numerical study to these models and clarify the relationship to the fermionic degrees of freedom.

ACKNOWLEDGMENTS

This work was partially supported by Grant-in-Aid for Scientific Research from Japan Society for the Promotion of Science under Grant No.26400246.

¹ I. Bloch, J. Dalibard, and W. Zwerger, *Rev. Mod. Phys.* **80**, 885 (2008); M. Lewenstein, A. Sanpera, and V. Ahufinger, *Ultracold Atoms in Optical Lattices: Simulating Quantum Many-body Systems* (Oxford University Press, Oxford, 2012).
² D. Jaksch, C. Bruder, J. I. Cirac, C. W. Gardiner, and P. Zoller: *Phys. Rev. Lett.* **81** (1998) 3108.
³ J. Dalibard, F. Gerbier, G. Juzeliunas, and P. Ohberg, *Rev. Mod. Phys.* **83**, 1523 (2011); M. Aidelsburger, M. Atala, M. Lohse, J. T. Barreiro, B. Paredes, and I. Bloch, *Phys. Rev. Lett.* **111**, 185301 (2013); H. Miyake, G. A. Siviloglou, C. J. Kennedy, W. C. Burton, and W. Ketterle, *Phys. Rev. Lett.* **111**, 185302 (2013); N. Goldman, G. Juzeliunas, P. Ohberg, and I. B. Spielman, *Rep. Prog. Phys.* **77** 126401 (2014).
⁴ G. Jotzu, M. Messer, R. Desbuquois, M. Lebrat, T. Uehlinger, D. Greif, and T. Esslinger, *Nature* **515**,

237 (2014).
⁵ F. D. M. Haldane, *Phys. Rev. Lett.* **61**, 2015 (1988).
⁶ I. Vasić, A. Petrescu, K. Le Hur, and W. Hofstetter, *Phys. Rev. B* **91**, 094502 (2015).
⁷ Y. Kuno, T. Nakafuji, and I. Ichinose, *Phys. Rev. A* **92**, 063630 (2015).
⁸ T. Nakafuji, T. Ito, Y. Nagamori, and I. Ichinose, *Phys. Rev. A* **94**, 023613 (2016).
⁹ C. N. Varney, K. Sun, V. Galitski, and M. Rigol, *Phys. Rev. Lett.* **107**, 077201 (2011); J. Carrasquilla, A. D. Ciolo, F. Becca, V. Galitski, and M. Rigol, *Phys. Rev. B* **88**, 241109 (2013).
¹⁰ T. Lahaye, C. Menotti, L. Santos, M. Lewenstein and T. Pfau, *Rep. Prog. Phys.* **72**, 126401 (2009).
¹¹ Y. Kuno, K. Suzuki, and I. Ichinose, *Phys. Rev. A* **90**, 063620 (2014).

- ¹² As we pointed out in the previous paper⁸, the coherent states $|\varphi_b\rangle$, $|\varphi_h\rangle$ contain multi-particle states even if they satisfy the local constraint such as $|\varphi_b|^2 + |\varphi_h|^2 = 1$. In most of cases, this fact does not matter to critical behaviors of many-body quantum systems if there are no frustrations. The term H_1 [Eq.(6)] suppresses the multi-particle states in the coherent state path integrals and has relevant physical meanings for systems with frustrations as in the present case.
- ¹³ N. Metropolis, A. W. Rosenbluth, M. N. Rosenbluth, A. M. Teller, and E. Teller, *J. Chem. Phys.* **21**, 1087 (1953); J. M. Thijssen, *Computational Physics* (Cambridge University Press, Cambridge, 1999).
- ¹⁴ See for example I. Montvay I and G. Muenster, *Quantum Fields on a Lattice* (Cambridge University Press, Cambridge, 1994).
- ¹⁵ R. F. Bishop, P. H. Y. Li, and C. E. Campbell, *Phys. Rev. B* **89**, 214413 (2014).
- ¹⁶ Y. Kuno, T. Mori, and I. Ichinose, *New J. Phys.* **16**, 083030, (2014).
- ¹⁷ C. N. Varney, K. Sun, M. Roigol, and V. Galitski, *Phys. Rev. B* **82**, 115125 (2010).
- ¹⁸ A. D. Ciolo, J. Carrasquilla, F. Becca, M. Rigol, and V. Galitski, *Phys. Rev. B* **89**, 094413 (2014).
- ¹⁹ C. N. Varney, K. Sun, V. Galitski, and M. Rigol, *New J. Phys.* **14**, 115028, (2012).
- ²⁰ Z. Zhu, D. A. Huse, and S. R. White, *Phys. Rev. Lett.* **111**, 257201 (2013).
- ²¹ T. A. Sedrakyan, L. I. Glazman, and A. Kamenev, *Phys. Rev. B* **89**, 201112 (2014); *Phys. Rev. Lett.* **114**, 037203 (2015); *Phys. Rev. A* **86**, 063639 (2012); T. A. Sedrakyan, V. M. Galitski, and A. Kamenev, *Phys. Rev. Lett.* **115**, 195301 (2015); *Phys. Rev. B* **95**, 094511 (2017).